Electrochemical Hydrogen Evolution: H^+ or H_2O Reduction?

A Rotating Disk Electrode Study

Vitali Grozovski[1], Soma Vesztergom*[2], Győző G. Láng[2], and Peter Broekmann†[1]

[1]University of Bern, Department of Chemistry and Biochemistry, Freiestrasse 3, 3012 Bern, Switzerland

[2]Eötvös Loránd University, Department of Physical Chemistry, Pázmány Péter sétány 1/A, 1117 Budapest, Hungary

Abstract

We study the effect of H^+ and OH^- diffusion on the hydrogen evolution reaction in unbuffered aqueous electrolyte solutions of mildly acidic pH values. We demonstrate that the cathodic polarization curves measured on a Ni rotating disk electrode in these solutions can be modelled by assuming two irreversible reactions, the reduction of H^+ and that of water

*vesztergom@chem.elte.hu (corresponding author)

†peter.broekmann@dcb.unibe.ch (corresponding author)

molecules, both following Erdey-Grúz–Volmer–Butler kinetics. The reduction of H^+ yields a transport-limited and thus, rotation rate-dependent current at not very negative potentials. At more cathodic potentials the polarization curves are dominated by the reduction of water and no mass transfer limitation seems to apply for this reaction. Although *prima facie* the two processes may seem to proceed independently, by the means of finite-element digital simulations we show that a strong coupling (due to the recombination of H^+ and OH^- to water molecules) exists between them. We also develop an analytical model that can well describe polarization curves at various values of pH and rotation rates. The key indication of both models is that hydroxide ions can have an infinite diffusion rate in the proximity of the electrode surface, a feature that can be explained by assuming a directed Grotthuss-like shuttling mechanism of transport.

1 Introduction

A common problem of base metal electroplating is that the deposition of electroactive metals (*e.g.*, Zn, Co, Fe or Ni) is almost inevitably accompanied by hydrogen evolution. In aqueous solutions hydrogen evolution always occurs if current is made high enough to exceed the limiting current of the deposited metal[1]. In acidic solutions hydrogen may be formed as a result of H^+ reduction,

$$H^+ + e^- \rightarrow \tfrac{1}{2}H_2, \tag{1}$$

while in solutions of $p\mathrm{H} > 7$, the primary source of hydrogen is the electroreduction of water itself:

$$\mathrm{H_2O} + \mathrm{e^-} \rightarrow \tfrac{1}{2}\mathrm{H_2} + \mathrm{OH^-}. \tag{2}$$

Hydrogen evolution presents several ramifications for electrochemical plating processes. From a strictly technological point of view, the evolution of hydrogen is a serious concern because it reduces the Faradaic efficiency of metal deposition, thereby increasing the amount of time and energy utilized to deposit the desired amount of metal at a given total current density. Another problem of hydrogen codeposition is that it can affect the structural and mechanical properties of the metal and can cause embrittlement [1].

Furthermore, hydrogen can also affect the kinetics of layer growth: if hydrogen adsorbs more efficiently on certain crystal planes of the metal, it may block these planes from further deposition so that the metal would preferentially grow on other planes [2]. This inhomogeneous growth presents difficulties for the deposition of compact metal layers at the best — that is, if the accumulated gas does not impair the entire plating process [1].

Finally, hydrogen evolution also results in the removal of $\mathrm{H^+}$ ions from the diffusion layer. Increasing the near-surface $p\mathrm{H}$ may alter the intended chemical and electrochemical reactions at the interface. For example, if the solution at the interface becomes sufficiently alkaline, it may cause the solubility of a hydroxide of the metal ion present to be exceeded, which may cause the inclusion of hydroxide or oxide species into the deposit [1,3]. This can be problematic in terms of deposit properties such as ductility and electrical resistivity. Alterna-

tively, hydroxide deposition could cause the formation of relatively thick films on plated parts, thus passivating the cathode surface[3–5]. While the accumulation of OH^- in the diffusion layer is usually negligible in sufficiently buffered solutions[6], severe changes may occur in unbuffered or only slightly buffered media[7].

From the point of view of base metal electroplating, the variation of local *p*H presents a challenge because it influences the kinetics of one of the most important side reactions, hydrogen evolution. However, the change of interfacial *p*H can, in general, affect all electrode reactions that involve H^+ or OH^- ions in their mechanisms[6–24]. Therefore, a great deal of research has aimed at the development of experimental methods for detecting local *p*H variations near an electrode surface. Most of these are either electrochemical or optical methods.

Optical methods usually involve the addition of a suitable *p*H indicator and detection by means of confocal laser scanning microscopy[13–15], an approach resulting in *p*H values averaged over a region in front of the electrode with a thickness depending on the spatial resolution of the instrument.

A straightforward way of electrochemical *p*H detection is to place a *p*H sensitive indicator electrode close to the working electrode surface[16–18]: as the indicator electrode is carefully positioned in the vicinity of the cathode, its potential is changed in response to the *p*H of its environment. This method is capable to map the variation of *p*H as a function of distance to the electrode surface if a precise positioning system is used such as in scanning electrochemical microscopy[19]. Although the indicator used in this approach is usually a

microelectrode, special care must be taken so that the indicator does not shield the flux of reacting species to the working electrode. In addition, the effect of IR drop must be taken into account[25,26]: that is, the method is only applicable when low cathode currents are flowing in a solution of low electrical resistance.

The problem of shielding, albeit not the problem of IR drop, can be efficiently circumvented by using the collector electrode of "generator–collector" systems in a potential sensing mode. Such experiments were described both for the rotating ring–disk electrode[20,21] and for the impinging jet cell geometries[22]. These methods are by nature not capable to "map" the pH profile near the cathode. However, by solving the diffusion-convection equations in the system, one can determine the pH in the vicinity of the working electrode based on the measured "collector" electrode potential. The detection of local pH changes immediately adjacent to the electrode surface during a redox reaction is, in addition, also possible by attaching a molecular pH probe to the cathode itself and carrying out generator–collector experiments using a single electrode[23,24].

As can be seen above, there is a variety of experimental techniques available for determining pH changes adjacent to an electrode surface. However, there are always some experimental difficulties present and most of these techniques cannot be used under *operando* conditions in a metal plating cell. Nonetheless, as hydrogen evolution is an ubiquitous side-reaction of metal deposition, a selective control of its rate as well as an understanding of its effects on the technological process are vital[1,3]. Hence, there is a strong need for understanding the kinetics of hydrogen evolution in solutions of different pH.

In this paper we use numerical simulations for modelling the hydrogen evolution reaction as it occurs on a nickel rotating disk electrode (RDE) immersed into strongly supported, unbuffered solutions of different *p*H values. The stationary polarization curves recorded in solutions of moderately acidic *p*H values show two characteristic sections: one associated with the electroreduction of H^+, Reaction (1), and another dominated by the electrolysis of water, Reaction (2)[27,28]. However, treating these processes independently is not a sound strategy of describing the overall mechanism due to the fast recombination of H^+, a reactant of Reaction (1) and OH^-, a product of Reaction (2):

$$H^+ + OH^- \rightleftharpoons H_2O. \tag{3}$$

Taking Reaction (3) into consideration is necessary not only to determine steady-state *p*H profiles corresponding to given electrode potentials[29], but also to account for the slight variation of the "limiting" H^+-reduction current with the electrode potential. This latter effect often causes inaccuracies in the determination of H^+ diffusion coefficients based on Levich- and Koutecký–Levich-like analyses[30,31]. As is going to be shown, finite element simulations can effectively model mass transfer to the electrode surface, even under the constraint of a strong chemical coupling[32]. By studying the results of finite element simulations and of actual experiments, we also develop an analytical model that can well-describe the measured polarization curves.

Interestingly, both digital simulation and the analytical model hint that OH^- ions, when present in the solution layers bounding the electrode surface have an infinitely large diffusion coefficient. This feature can be explained by assuming

what we call a "directed Grotthuss mechanism" of transport.

2 Experimental

The disk-shaped polycrystalline nickel electrode (diameter: 5 mm) used in this work was obtained from MaTeck and was embedded in a PTFE shroud (external diameter: 1.2 cm) to form an RDE tip. Prior to the experiments the electrode surface was mirror-polished by using a diamond suspension of ≤ 0.01 µm grain size. In order to further decrease the surface roughness, the electrode was made subject to electrochemical polishing in a 50% aqueous H_3PO_4 solution at a current density of ~ 1 A cm^{-2}. Prior to use, the electrode was rinsed abundantly with Milli-Q water ($R = 18.2$ MΩ cm, used for the preparation of solutions as well).

The studied solutions of different pH were prepared from 0.1 mol dm^{-3} $HClO_4$ (70%, Merck, Suprapure) and 0.1 mol dm^{-3} KOH (Sigma Aldrich, Semiconductor grade). The solutions were mixed until the desired pH was reached. The pH of the solution was measured by a calibrated Metrohm 744 pH meter. Each solution was boiled prior to the experiment for 30 minutes in order to remove any carbonate contamination. Later on, the solution volume was corrected by taking into account the evaporated amount of water and the pH was fine-adjusted.

A lab-made hermetic three-electrode glass cell with a large Pt counter electrode and a Ag | AgCl | 3 mol dm^{-3} KCl reference electrode (connected to

the main chamber through Luggin capillary), was used in this work. Prior to measurements, the solution in the cell was deaerated with a pure Ar flow (5N, Alphagaz).

The Ni working electrode was submerged to the electrolyte solution while maintaining its potential at an "inert" E_{init} value where no current flows. (These values are typically between -400 and -600 mV vs. Ag | AgCl.) Polarization curves presented in the paper were recorded point-by-point by steady-state current measurements at given electrode potentials and rotation rates, according to the following sequence: the electrode potential and the rotation rate were set, and the current was measured until it reached a stationary value. Then the potential was set back to E_{init} and a rotation rate of $f = 2500$ min^{-1} was applied for 30 s in order to remove any accumulated H_2 from the surface. The current measurement was then repeated with other potential and rotation rate settings. The measured data were IR-corrected post-experimentally — the solution resistance can be determined by means of high-frequency impedance measurements.

The measurements were automated by using an Autolab PGSTAT128N potentiostat in connection with a PINE AFMSRCE rotator and by the application of the Nova v11.0 software.

3 Results

Stationary polarization curves recorded on a Ni RDE show a strong pH dependence (Figure 1). In case of $p\mathrm{H} \lesssim 1.5$ the measured current is almost entirely dominated by the reduction of H^+, Reaction (1), and due to the high H^+ concentration there is hardly any mass transfer limitation to this electrode reaction. On the other hand, in case of $p\mathrm{H} \gtrsim 3.0$ (very low H^+ concentration) practically no H^+ reduction can be measured: significant currents are only yielded by the reduction of water, Reaction (2), at very negative potentials.

In case of mildly acidic pH values ($2 \lesssim p\mathrm{H} \lesssim 3$) the afore-mentioned reactions both play a significant role in determining the shape of stationary polarization curves. From positive to negative electrode potentials, the polarization curves recorded at mildly acidic pH values start with a more-or-less exponential section where the current, due to the reduction of H^+, is limited by charge transfer. At more cathodic overpotentials the rate of charge transfer increases and the measured current is limited more and more by the transport of H^+ from the bulk of the electrolyte solution to the electrode interface. As mass transfer becomes the only limiting step, the stationary polarization curves exhibit an almost but not quite horizontal limiting current section. The limiting current is in reasonable agreement with predictions of the Levich equation[33], see Figure 2:

$$j_{\ell,\mathrm{H}^+} = -0.620 F D_{\mathrm{H}^+}^{2/3} \omega^{1/2} \nu^{-1/6} c_{\mathrm{H}^+}^{\infty}, \tag{4}$$

where D_{H^+} is the diffusion coefficient and $c_{\mathrm{H}^+}^{\infty}$ is the bulk concentration of H^+

ions, $\omega = 2\pi f$ is the angular frequency of rotation and ν is the kinematic viscosity of the solution. As the overpotential exceeds the limiting current section in the negative direction, the cathodic current increases again due to the reduction of water molecules, Reaction (2).

With respect to Figures 1 and 2, the following comments are of relevance: *i.)* The shape of the polarization curves, especially at more cathodic potentials, remain essentially unchanged when the measurement is carried out in a solution saturated with H_2 gas. This leads us to assume irreversible kinetics (*i.e.*, the rate of Reactions (1) and (2) in the backward direction is negligible). *ii.)* The limiting current sections of the polarization curves recorded in solutions of mildly acidic *p*H values are not perfectly constant but show a slight dependence on the electrode potential (this is best shown in Figure 2).

In order to describe the measured polarization curves we shall, in what follows, attempt to develop two models that describe the kinetics of the studied electrode process where both the reduction of H^+ ions and the reduction of water molecules play a significant role in determining the current. As a first step we devise a numerical method for the simulation of the electrode process; then, based on the results of numerical simulations, we develop an analytical model that can explain the behaviour of the system under study and that can even be used for the fitting of measured polarization curves and for the determination of kinetic parameters.

4 Modelling

We start with the simplifying assumption that Reactions (1) and (2) both follow Erdey-Grúz–Volmer–Butler kinetics[34] and the currents yielded by these reactions can be described as

$$j_1 = -Fk_1 c^0_{\mathrm{H^+}} \exp\left(-\frac{\alpha_1 F}{RT}\left(E - E_1^{\mathrm{eq}}\right)\right) \tag{5.a}$$

and

$$j_2 = -Fk_2 \exp\left(-\frac{\alpha_2 F}{RT}\left(E - E_2^{\mathrm{eq}}\right)\right), \tag{5.b}$$

where k_i is the rate coefficient, α_i is the charge transfer coefficient and E_i^{eq} is the equilibrium potential of the i^{th} electrode reaction (Reaction (1) or (2)). In Equation (5.a), $c^0_{\mathrm{H^+}}$ denotes the near-surface concentration of $\mathrm{H^+}$ ions. Here we note that with this assumption we only wish to state that there exists an exponential dependence between the stationary partial currents and the electrode potential[35]; in what follows we shall not draw any conclusion whatsoever about the exact mechanism of hydrogen evolution (and whether it follows a "pure" Volmer, a Volmer–Heyrovsky or a Volmer–Tafel mechanism[35]).

In order to determine steady state currents one has to assume that the concentration of $\mathrm{H^+}$ and $\mathrm{OH^-}$ ions in the system is stationary, thus

$$\begin{aligned}\frac{\partial c_{\mathrm{H^+}}}{\partial t} &= D_{\mathrm{H^+}}\nabla^2 c_{\mathrm{H^+}} - \boldsymbol{v}\cdot\nabla c_{\mathrm{H^+}} - k_{+3}c_{\mathrm{H^+}}c_{\mathrm{OH^-}} + k_{-3} \\ &= 0\end{aligned} \tag{6.a}$$

and

$$\frac{\partial c_{\mathrm{OH^-}}}{\partial t} = D_{\mathrm{OH^-}} \nabla^2 c_{\mathrm{OH^-}} - \boldsymbol{v} \cdot \nabla c_{\mathrm{OH^-}} - k_{+3} c_{\mathrm{H^+}} c_{\mathrm{OH^-}} + k_{-3}.$$
$$= 0 \tag{6.b}$$

Here $\boldsymbol{v}$ denotes the vector field of (stationary) fluid flow, and the symbols k_{+3} and k_{-3} were introduced to denote the forward and backward rate coefficients of Reaction (3), respectively. It was assumed at this point that mass transfer occurs only by means of diffusion and convection, while other means of transport (*e.g.*, migration) are ignored. It was further assumed that the diffusion coefficients $D_{\mathrm{H^+}}$ and $D_{\mathrm{OH^-}}$ are constants, independent of the concentrations and of spatial coordinates.

Assuming that the radius of the disk electrode is appropriately big, the effect of transport in the radial direction can be neglected[36] and thus instead of solving the partial differential Equations (6.a)–(6.b), a solution of the set of ordinary differential equations

$$D_{\mathrm{H^+}} \frac{\mathrm{d}^2}{\mathrm{d}\, z^2} c_{\mathrm{H^+}}(z) + k_{-3} = v_z \frac{\mathrm{d}}{\mathrm{d}\, z} c_{\mathrm{H^+}}(z) + k_{+3} c_{\mathrm{H^+}}(z) c_{\mathrm{OH^-}}(z) \tag{7.a}$$
$$D_{\mathrm{OH^-}} \frac{\mathrm{d}^2}{\mathrm{d}\, z^2} c_{\mathrm{OH^-}}(z) + k_{-3} = v_z \frac{\mathrm{d}}{\mathrm{d}\, z} c_{\mathrm{OH^-}}(z) + k_{+3} c_{\mathrm{H^+}}(z) c_{\mathrm{OH^-}}(z). \tag{7.b}$$

is sufficient. Here we invoke the usual assumption[37] that in the vicinity of the electrode plane the magnitude of fluid flow in the axial direction can be approximated as

$$v_z = -B z^2 \sqrt{\frac{\omega^3}{\nu}}, \tag{8}$$

where $B = 0.51$. Higher terms in Equation (8) are ignored here for the sake of simplifying the analytical solution presented in Section 4.2. Due to the finiteness

of the Schmidt-number in the system, this introduces an $\sim 3\%$ error to the calculation of the limiting current [38].

Due to the kinetic (chemical) coupling terms they contain, Equations (7.a)–(7.b) describe a strongly non-linear system of ordinary (inhomogeneous) differential equations that cannot be solved by direct integration. In what follows we present a few approximate solutions by means of analytical and of numerical approaches.

4.1 Numerical Solution of the Equations of Transport under the Constraint of Chemical Coupling

It is a very plausible assumption that the recombination of H^+ and OH^- ions in Reaction (3) is an extremely fast process and dictates instantaneous equilibrium. This fast pre-equilibrium assumption enables us to get a numerical solution of Equations (7.a)–(7.b) by the application of a constraint to the concentration of H^+ and OH^- ions, namely that

$$c_{H^+} c_{OH^-} = K_w c^{\ominus 2} = 10^{-14} \text{ mol}^2 \text{ dm}^{-6}. \tag{9}$$

Here $K_w = 10^{-14}$ is the (by definition, dimensionless) autoprotolysis constant of water and $c^{\ominus} = 1$ mol dm^{-3} is the standard concentration. Note that with Equation (9) we assume unit activities for the H^+ and OH^- ions.

In the finite element simulations we tile the space under the RDE in the z direction to an n number of small volumes (cylinders of height Δz). Accordingly, the concentrations of H^+ and OH^- ions will be ordered into one-dimensional

arrays (of size n, denoted by $\mathsf{c}_{\mathrm{H^+}}$ and $\mathsf{c}_{\mathrm{OH^-}}$) so that the i^{th} entry of each array corresponds to the respective concentration in the i^{th} small cylinder counted from the electrode surface.

The simulation starts from a state when both $\mathrm{H^+}$ and $\mathrm{OH^-}$ are evenly distributed, thus for every i

$$\mathsf{c}_{\mathrm{H^+}_i} = c^{\infty}_{\mathrm{H^+}} \tag{10.a}$$

and

$$\mathsf{c}_{\mathrm{OH^-}_i} = \frac{K_{\mathrm{w}} c^{\ominus\,2}}{c^{\infty}_{\mathrm{H^+}}}. \tag{10.b}$$

In every step of the simulation (corresponding to a time interval of Δt) new $\mathsf{c}_{\mathrm{H^+}}$ and $\mathsf{c}_{\mathrm{OH^-}}$ arrays are calculated. To do this, we "update" the array entries as described in what follows (the operator ":=" in the following equations means that "updated" arrays are calculated using "present" concentration values).

1. **Realization of charge transfer.** Charge transfer affects only the first elements of the concentration arrays; that is,

$$\mathsf{c}_{\mathrm{H^+}_1} := \mathsf{c}_{\mathrm{H^+}_1} \exp\left(\frac{-b_1 \Delta t}{\Delta z}\right) \tag{11.a}$$

and

$$\mathsf{c}_{\mathrm{OH^-}_1} := \mathsf{c}_{\mathrm{OH^-}_1} + \frac{b_2 \Delta t}{\Delta z}, \tag{11.b}$$

where $b_1 = k_1 \exp\left(-\frac{\alpha_1 F}{RT}\left(E - E_1^{\mathrm{eq}}\right)\right)$ and $b_2 = k_2 \exp\left(-\frac{\alpha_2 F}{RT}\left(E - E_2^{\mathrm{eq}}\right)\right)$.

2. **Realization of mass transport.** The effect of mass transfer is realized in each simulation step by using the (explicit) Euler method[39] described by

the following matrix-vector equations:

$$\mathsf{c}_{\mathrm{H^+}} := (\mathsf{I} + \mathsf{V})\,(\mathsf{I} + D_{\mathrm{H^+}}\mathsf{D})\,\mathsf{c}_{\mathrm{H^+}} \tag{12.a}$$

and

$$\mathsf{c}_{\mathrm{OH^-}} := (\mathsf{I} + \mathsf{V})\,(\mathsf{I} + D_{\mathrm{OH^-}}\mathsf{D})\,\mathsf{c}_{\mathrm{OH^-}} \tag{12.b}$$

where the I identity, D diffusor and V conveyor operators are all $n \times n$ matrices defined as:

$$\mathsf{I}_{i,k} = \begin{cases} 1 & \text{if } i = k \\ 0 & \text{otherwise} \end{cases} \tag{13}$$

$$\mathsf{D}_{i,k} = \begin{cases} -\frac{2\Delta t}{\Delta z^2} & \text{if } i = k \\ \frac{\Delta t}{\Delta z^2} & \text{if } i = k \pm 1 \\ 0 & \text{otherwise} \end{cases} \tag{14}$$

$$\mathsf{V}_{i,k} = \begin{cases} -\left(i - \frac{1}{2}\right)^2 \Delta z \Delta t B \sqrt{\frac{\omega^3}{\nu}} & \text{if } i = k \\ \left(i - \frac{1}{2}\right)^2 \Delta z \Delta t B \sqrt{\frac{\omega^3}{\nu}} & \text{if } i = k - 1 \\ 0 & \text{otherwise} \end{cases} \tag{15}$$

3. Recombination of ions. In order to account for the recombination of $\mathrm{H^+}$ and $\mathrm{OH^-}$ ions according to Reaction (3), the following algebraic equation is solved for every i entry of the concentration arrays:

$$\left(\mathsf{c}_{\mathrm{H^+}_i} - x_i\right)\left(\mathsf{c}_{\mathrm{OH^-}_i} - x_i\right) = K_{\mathrm{w}} c^{\ominus\,2}. \tag{16}$$

Then, using the physically relevant x_i roots only,

$$\mathsf{c}_{\mathrm{H^+}_i} := \mathsf{c}_{\mathrm{H^+}_i} - x_i \tag{17.a}$$

and

$$\mathsf{c}_{\mathrm{OH^-}_i} := \mathsf{c}_{\mathrm{OH^-},i} - x_i \tag{17.b}$$

After setting the electrode potential E to the desired value, the above iteration is run until convergence is reached; *i.e.*, until the concentration profiles become stationary. Note that step 3 assures that the product of $\mathsf{c}_{\mathrm{H^+}_i}$ and $\mathsf{c}_{\mathrm{OH^-}_i}$ entries is in accordance with the autoprotolysis constant at every i index: thus, by means of this method, one can determine a single pH profile as opposed to two "independent" profiles for $\mathrm{H^+}$ and $\mathrm{OH^-}$. Current, as usual in digital simulation [40], is calculated by approximating the near-surface concentration gradients with finite differences. This yields two partial current densities,

$$j_{\mathrm{H^+}} = \frac{F D_{\mathrm{H^+}}}{\Delta z} \left(\mathsf{c}_{\mathrm{H^+}_2} - \mathsf{c}_{\mathrm{H^+}_1} \right) \tag{18.a}$$

and

$$j_{\mathrm{OH^-}} = - \frac{F D_{\mathrm{OH^-}}}{\Delta z} \left(\mathsf{c}_{\mathrm{H^+}_2} - \mathsf{c}_{\mathrm{H^+}_1} \right), \tag{18.b}$$

the sum of which gives the total current density j.

Results of two different simulations (polarization curves and pH profiles corresponding to various electrode potential values) are presented in Figure 3 for the case of $p\mathrm{H} = 2.0$ and $f = 900$ min^{-1}. We used the same parameter set listed in Table 1 in both simulations, except that we assumed different values

for the diffusion coefficient of hydroxide ions, $D_{\mathrm{OH^-}}$. When calculating the polarization curve shown in Figure 3(a) and the pH profiles shown in Figure 3(b) we assumed that the $\beta = D_{\mathrm{OH^-}}/D_{\mathrm{H^+}}$ ratio is small, having a value of 0.5, as suggested by literature[30]. On the other hand, the polarization curve seen in Figure 3(c) and the pH profiles of Figure 3(d) were simulated using a much larger value of $\beta = 2 \cdot 10^4$.

It is apparent in Figure 3(a) and (c) that regardless of the value of β there is a good agreement between measured and simulated currents up until the point where the electrode potential exceeds the limiting current region. Currents measured at this potential range seem to be in accordance with the Koutecký–Levich-equation[37]:

$$j_{\mathrm{H^+}} = \left(\frac{1}{j_{\ell,\,\mathrm{H^+}}} + \frac{1}{j_{\mathrm{cat},\,\mathrm{H^+}}} \right)^{-1}, \tag{19}$$

where $j_{\ell,\,\mathrm{H^+}}$ is defined by Equation (4) and

$$j_{\mathrm{cat},\,\mathrm{H^+}} = -F k_1 c^{\infty}_{\mathrm{H^+}} \exp\left(-\frac{\alpha_1 F}{RT} \left(E - E_1^{\mathrm{eq}} \right) \right). \tag{20}$$

In the $\beta \approx 0.5$ case, Figure 3(a), a big deviation appears between the simulated polarization curve and the measured currents at electrode potentials below the limiting current region. At potentials less than -1.4 V the reduction of water molecules already yields a significant current (Equation (5.b)), which at approximately -1.6275 V surpasses the limiting current of $\mathrm{H^+}$ reduction. This potential marks a strong transition in the polarization curve: as shown in Figure 3(b), at approximately -1.6275 V the near-surface pH reaches the value of 7, the flux of $\mathrm{H^+}$ ions drops to practically zero and the total current becomes

entirely dominated by the gradient of OH^-.

The situation is somewhat different when the assumption of $\beta \gg 1$ is applied, see Figures 3(c) and 3(d). Now the diffusion coefficient of OH^- is large and this expands the effect of autoprotolysis within the solution layer. As a result, pH values at the electrode surface are nivellated (tend to be closer to neutral), however the "reaction layer"[41] is essentially broader than it was in the case of $\beta < 1$.

In case when $\beta \gg 1$, simulated current densities are in a closer agreement with measured data and the transition of partial currents is much smoother than it was in the previous case.

It is worth to note in Figure 3(c) that the partial current calculated from the gradient of OH^- already gives a significant contribution to the overall current at potentials when the rate of water reduction is still very small. This is due to the autoprotolysis process which in case of $\beta \gg 1$ can assure that any near-surface decrease of the H^+ concentration would ultimately lead to an increase of c_{OH^-}.

Although the numerical simulation described above is in agreement with measured data, the numerical model by nature cannot give an analytical formula that could be used for the fitting of measured polarization curves and for the quick determination of reaction parameters. Therefore, in what follows we attempt to describe the problem using an analytical approximation.

4.2 Approximate Analytical Solution of the Transport Problem with the Constraint of Chemical Coupling

The ordinary differential Equations (7.a)–(7.b) could not be solved analytically due to a strong non-linear coupling introduced by the autoprotolysis process, Equation (3). In the previous section we discussed that the upper segments of the measured polarization curves (at potentials more positive than the limiting current section) can well be described by the simple Koutecký–Levich equation (19), and we saw that problems start to arise when the flux of OH^- ions also gives a significant contribution to the measured current.

In what follows we describe an essentially analytical model of the problem that tries to circumvent the non-linearity introduced by Reaction (3). We will assume that at very cathodic potentials where both H^+ and OH^- ions have a role in determining the current density, the solution layer close to the interface can be divided into two parts. In one part, closer to the surface, only OH^- ions can exist in the solution, while in the other part further away, only H^+ ions are present. The two regimes are separated by a "reaction plane" at a distance λ measured from the surface, acting as a sink for both ions.

This scenario, which is somewhat similar to that described by Chapman[42,43] for other reacting systems, assumes that within the two distinct regimes the concentrations of the ions obey the general convection/diffusion equation of the form

$$D_i \frac{\mathrm{d}^2}{\mathrm{d}\,z^2} c_i(z) = v_z \frac{\mathrm{d}}{\mathrm{d}\,z} c_i(z). \tag{21}$$

Here the index i stands for the species H^+ and OH^-, and the differential equation has to be solved for both ions.

First we note that the general solution [37] of the ordinary differential equation (21) is a function of the form

$$c_i(z) = \chi_{2,i} - \frac{1}{3} z \chi_{1,i} \, \mathrm{Ei}_{2/3}\left(\frac{B z^3 \omega^{3/2}}{3 D_i \nu^{1/2}}\right), \tag{22}$$

where $\chi_{1,i} = \lim_{z\to 0}\left(\frac{\mathrm{d}}{\mathrm{d}\,z} c_i(z)\right)$ and $\chi_{2,i} = \lim_{z\to\infty}(c(z))$ are integration constants and the $\mathrm{Ei}_s(x)$ exponential integral function is defined as

$$\mathrm{Ei}_s(x) = \int_1^\infty \frac{\exp(-xu)}{u^s}\,\mathrm{d}\,u. \tag{23}$$

Then, in order to get appropriate particular solutions we formulate five boundary conditions, four fixing the values of the integration constants and a fifth defining the reaction plane position λ. The five boundary conditions are as follows:

i.) As $z \to \infty$ the concentration of H^+ ions tends to the bulk H^+ concentration and the concentration of OH^- vanishes. Thus,

$$\chi_{2,H^+} = c^\infty_{H^+} \tag{23.a}$$

and

ii.)

$$\chi_{2,OH^-} = 0. \tag{23.b}$$

iii.) The gradient of the OH^- concentration at $z \to 0$ is, according to Fick's first law, determined by the j_2 current density defined in Equation (5.b).

Thus,

$$\chi_{1,\mathrm{OH^-}} = \frac{j_2}{F D_{\mathrm{OH^-}}}. \tag{23.c}$$

iv.) At $z = \lambda$, there is an equal concentration of H^+ and OH^- ions. From this follows that

$$\chi_{1,\mathrm{H^+}} = \frac{3 c^{\infty}_{\mathrm{H^+}} F D_{\mathrm{OH^-}} + j_2 \lambda \,\mathrm{Ei}_{2/3}\left(\frac{B\lambda^3\omega^{3/2}}{3D_{\mathrm{OH^-}}\nu^{1/2}}\right)}{F D_{\mathrm{OH^-}} \lambda \,\mathrm{Ei}_{2/3}\left(\frac{B\lambda^3\omega^{3/2}}{3D_{\mathrm{H^+}}\nu^{1/2}}\right)}. \tag{23.d}$$

v.) Finally, at $z = \lambda$, the sum of the fluxes of the two species must be zero. This gives the following transcendental equation defining λ:

$$\begin{aligned}\lambda =& \frac{3 c^{\infty}_{\mathrm{H^+}} F D_{\mathrm{H^+}} D_{\mathrm{OH^-}}}{j_2} \Bigg/ \Bigg(\exp\left[\frac{B\left(D_{\mathrm{OH^-}} - D_{\mathrm{H^+}}\right)\lambda^3\omega^{3/2}}{3 D_{\mathrm{H^+}} D_{\mathrm{OH^-}} \nu^{1/2}}\right] D_{\mathrm{OH^-}} \\ & \mathrm{Ei}_{2/3}\left[\frac{B\lambda^3\omega^{3/2}}{3D_{\mathrm{H^+}}\nu^{1/2}}\right] + D_{\mathrm{H^+}}\,\mathrm{Ei}_{2/3}\left[\frac{B\lambda^3\omega^{3/2}}{3D_{\mathrm{OH^-}}\nu^{1/2}}\right]\Bigg)\end{aligned} \tag{23.e}$$

Now at this point it is already possible to determine the value of λ from Equation (23.e), *e.g.*, by the Newton–Raphson method[39] of iterative root-finding. After obtaining a numerical value of λ, the integration constants can be determined from Equations (23.a)–(23.d) and substituted into the general solution given by Equation (22) to obtain stationary concentration profiles for both H^+ and OH^-.

In Figure 4 we compare H^+ and OH^- concentration profiles determined by the method of digital simulation, described in Section 4.1, and by the quasi-analytical approach presented here. Figure 4(a) shows that in case of $\beta < 1$ the analytical method yields concentration profiles that do not match those obtained by digital simulation. This is due to the boundary conditions of the

model which assure the equality of concentrations and the cancellation of fluxes at λ but they fail to maintain the chemical constraint dictated by Reaction (2) that at the distance λ both concentrations should have a very low value. As the results of digital simulations suggest, however, we are primarily interested in an analytical solution that is valid for the $\beta \gg 1$ case, and this condition in itself will assure zero concentrations at the reaction plane. Thus, in a $\beta \gg 1$ case we can expect better agreement between the simulated and analytically approximated curves, as it is also shown in Figure 4(b) and (c).

The assumption that $\beta \gg 1$ also has implications on the analytical model, and this assumption is a step forward to obtain closed-form expressions for the concentration profiles and the current density. First, by using the substitution $D_{\mathrm{OH^-}} = \beta D_{\mathrm{H^+}}$ in Equation (23.e) and then taking the $\beta \to \infty$ limit of the right-hand side, we arrive to the following expression containing λ:

$$1 + \frac{3^{2/3} F B^{1/3} \omega^{1/2} c^{\infty}_{\mathrm{H^+}} D^{2/3}_{\mathrm{H^+}}}{j_2 \nu^{1/6} \exp\left(\frac{B\lambda^3\omega^{3/2}}{3D_{\mathrm{H^+}}\nu^{1/2}}\right) \Gamma_{1/3}\left(\frac{B\lambda^3\omega^{3/2}}{3D_{\mathrm{H^+}}\nu^{1/2}}\right)} = 0, \tag{24}$$

where $\Gamma_s(x)$ denotes the (upper) incomplete gamma function defined as

$$\Gamma_s(x) = \int_x^{\infty} u^{s-1} \exp(-u)\, \mathrm{d}\, u. \tag{25}$$

Equation (24) is still a transcendental equation, solving it by means of an analytical approximation is however possible. First we note that Equation (24) contains the functions $\exp(x)$ and $\Gamma_{1/3}(x)$ with the same argument $x = \frac{B\lambda^3\omega^{3/2}}{3D_{\mathrm{H^-}}\nu^{1/2}}$, and that for the system under study (cf. to the results of digital simulation), $x \gg 1$. Thus, by using the asymptotic approximation[44] that $\exp(x)\Gamma_s(x) \approx x^{s-1}$ in Equation (24), we arrive to the following approximative closed-form

expression defining λ:

$$\lambda = \sqrt[4]{\frac{\nu}{\omega^3}} \sqrt{\frac{-j_2}{BFc^{\infty}_{\mathrm{H^+}}}}. \tag{26}$$

As shown in Figure 4(b) and (c), H^+ concentration profiles calculated from a λ value defined by Equation (26) agree well with profiles created by digital simulations assuming that $\beta \gg 1$. Note that the analytical model yields an OH^- concentration of zero for the $0 \leq z \leq \lambda$ range where the OH^- concentration determined by digital simulation is also small. Accordingly, at the distance λ the H^+ concentration starts to rise from a value of 0, and this is consistent with the behaviour of the H^+ profile obtained by simulation.

In Figure 4(c), where the electrode potential (and thus j_2) is not very negative, the value of λ is negligibly small, and the current density, as calculated from the near-surface gradient of the H^+ profile, is almost exactly identical to the limiting current density $j_{\ell,\mathrm{H^+}}$. As shown in Figure 4(b), at more negative potentials λ grows larger and the electrode is covered with a seemingly "neutral" solution layer. In this case the current density can be calculated from the gradient of the H^+ profile at the distance λ. This enhanced current density $j^{\dagger}$ can be given as

$$j^{\dagger} = -\frac{3c^{\infty}_{\mathrm{H^+}} F D_{\mathrm{H^+}} \exp\left(-\frac{B\lambda^3\omega^{3/2}}{3D_{\mathrm{H^+}}\nu^{1/2}}\right)}{\lambda \,\mathrm{Ei}_{2/3}\left(-\frac{B\lambda^3\omega^{3/2}}{3D_{\mathrm{H^+}}\nu^{1/2}}\right)}. \tag{27}$$

It can be shown that if the applied electrode potential is not very negative, the value of $j^{\dagger}$ tends to $j_{\ell,\mathrm{H^+}}$ while at very negative potentials $j^{\dagger} \approx j_2$. Thus the *entire* polarization curve can be described as

$$j = j^{\dagger} - \frac{j^2_{\ell,\,\mathrm{H^+}}}{j_{\ell,\,\mathrm{H^+}} + j_{\mathrm{cat},\,\mathrm{H^+}}}, \tag{28}$$

which is a closed-form expression of the potential through Equations (4), (5.b), (20) and (27), when λ is defined as in Equation (26).

The analytical expression of Equation (28) can be used quite efficiently for the estimation of parameters in non-linear curve fitting, as it is shown in Figure 5. The parameter values used for the simulation of curves are those listed in Table 1. In case of certain parameters (such as the T temperature and the ν kinematic viscosity), values were assumed and not varied during the iteration. The equilibrium potentials E_1^{eq} and E_2^{eq} were determined from the Nernst-equation

$$E_i^{\mathrm{eq}} = E_i^{\ominus} - 0.059 p\mathrm{H}. \tag{29}$$

Here $E_1^{\ominus} = -0.225$ V vs. Ag|AgCl and $E_2^{\ominus} = -1.0502$ V vs. Ag|AgCl are the standard potentials corresponding to electrode reactions (1) and (2), respectively. A constant partial pressure of $p_{\mathrm{H_2}} = p^{\ominus} = 1$ bar was assumed.

In the non-linear fitting process, the $\mathrm{H^+}$ concentration, the diffusion coefficient of $\mathrm{H^+}$ and the reaction rate parameters (k_1, α_1, k_2 and α_2) were varied. The optimized concentrations are not far from those approximated from the pH and the diffusion coefficient of $\mathrm{H^+}$ matches its commonly accepted literature value[30]. The determined kinetic parameters are in alignment with those reported earlier for $\mathrm{H^+}$ reduction on Ni electrodes[35].

5 Discussion

In the previous section we devised two models (one based on digital simulation, another on analytical approximation) for the description of hydrogen evolution

in solutions of mildly acidic *p*H values where both H^+ reduction and the reduction of water molecules play a significant role in determining the current.

Based on the analytical model it became possible to determine kinetic and transport parameters of the hydrogen evolution process by means of non-linear curve fitting (Figure 5). The determined parameters (Table 1), when used in the simulation-based model, also yielded polarization curves that agree well with measured data (Figure 3). It is very interesting to note, however, that both models seem to "work well" (*i.e.*, comply to measurements) only when the *apparent* diffusion coefficient of OH^- is assumed to be very large. This property of the models deserves further explanation.

First of all we have to emphasize that D_{OH^-} in our interpretation, when used in Fick's equation of transport is indeed an *apparent* diffusion coefficient and thus special care must be taken when we compare it to literature values. In literature D_{OH^-} is traditionally determined by small-signal perturbations in a near-equilibrium system, *e.g.*, by *ac* conductivity measurements in an alkaline solution. Implicitly utilizing the fluctuation-dissipation theorem, the aim of such experiments is to give a good measure of the diffusion coefficient as it appears, for example, in the theory of random walk. D_{OH^-}, when determined from these experiments is reasonably small (approximately one-half of the diffusion coefficient of H^+ ions,[45]) but it is, again, characteristic to a near-equilibrium system.

The case studied in this paper is very different, and it is not even close to equilibrium. In our case OH^- ions created at the electrode surface by the

reduction of H_2O are separated from the acidic bulk only by a very thin neutral solution layer, having a thickness not bigger than a few tens of micrometers. Within this scheme one can assume that the driving force of transport is very big, and that the increased diffusivity of OH^- can be explained by what we call a "directed Grotthuss mechanism". The Grotthuss mechanism —even in case when small-signal perturbations are applied to a system— is known to be responsible for the enhanced diffusivity of OH^- compared to other ions of similar size[46]. We believe, however, that this mechanism can account for an even faster transport between the close-to-neutral electrode surface and an acidic solution region not far away from it; then, as illustrated by Figure 6, instead of a displacement of OH^- ions a shuttling of chemical bonds would be responsible for the very large value of D_{OH^-}. A similar effect was already reported for the interdiffusion of acids and bases[47] and, more recently, in theoretical studies dealing with OH^- diffusion in nanoconfined spaces[48].

6 Conclusion

In this paper we studied hydrogen evolution as it occurs in unbuffered, mildly acidic aqueous electrolyte solutions on a Ni RDE. We demonstrated that the cathodic polarization curves measured in these solutions can be modelled by assuming two irreversible reactions, the reduction of H^+ and that of water molecules.

By the means of finite-element digital simulations we showed that a strong

coupling (due to the recombination of H^+ and OH^- to water molecules) exists between the two processes. We also developed an analytical model that could well describe polarization curves at various values of *p*H and rotation rates and that can also serve as a good basis for more detailed studies of the mechanism, *e.g.*, by means of impedance spectroscopy.

The key indication of both models is that hydroxide ions can have an infinite diffusion rate in the proximity of the electrode surface, a feature we explained by assuming a directed Grotthuss-like shuttling mechanism of transport.

Acknowledgement

This research was supported by the European Union and the State of Hungary, co-financed by the European Social Fund in the framework of TÁMOP 4.2.4.A/1–11–1–2012–0001 "National Excellence" Program. G.G. Láng gratefully acknowledges support from the Hungarian Scientific Research Fund (OTKA–K109036). P. Broekmann acknowledges financial support by the Swiss National Science Foundation (SNSF–200020–149224/1).

References

References

[1] M. Schlesinger and M. Paunovic, eds., *Modern Electroplating*, Wiley, New York, 5 edition (2010).

[2] E. Chassaing, M. Jousselin and R. Wiart, *J. Electroanal. Chem.*, **157**, 75 (1983).

[3] N. R. Ritzert and T. P. Moffat, *J. Phys. Chem. C*, **120**, 27478 (2016).

[4] F. Ovari and A. L. Rotinjan, *Sov. Electrochem.*, **6**, 516 (1970).

[5] H. Göhr and H. Krüger, *Electrochim. Acta*, **11**, 835 (1966).

[6] T. Shinagawa and K. Takanabe, *J. Phys. Chem. C*, **119**, 20453 (2015).

[7] I. Katsounaros, J. C. Meier, S. O. Klemm, A. A. Topalov, P. U. Biedermann, M. Auinger and K. J. J. Mayrhofer, *Electrochem. Commun.*, **13**, 634 (2011).

[8] A. T. Kuhn and C. Y. Chan, *J. Appl. Electrochem.*, **13**, 189 (1983).

[9] M. M. Tlili, M. Benamor, C. Gabrielli, H. Perrot and B. Tribollet, *J. Electrochem. Soc.*, **150**, 765 (2003).

[10] C. Batchelor-McAuley, Q. Li, S. M. Dapin and R. G. Compton, *J. Phys. Chem. B*, **114**, 4094 (2010).

[11] S.-X. Guo, S. W. Feldberg, A. M. Bond, D. L. Callahan, P. J. S. Richardt and A. G. Wedd, *J. Phys. Chem. B*, **109**, 20641 (2005).

[12] M. Z. Southard, D. W. Green, V. J. Stella and K. J. Himmelstein, *Pharm. Res.*, **9**, 58 (1992).

[13] S. Cannan, I. D. Macklam and P. R. Unwin, *Electrochem. Commun.*, **4**, 886 (2002).

[14] N. C. Rudd, S. Cannan, E. Bitziou, I. Ciani, A. L. Whitworth and P. R. Unwin, *Anal. Chem.*, **77**, 6205 (2005).

[15] A. J. Leenheer and H. A. Atwater, *J. Electrochem. Soc.*, **159**, 752 (2012).

[16] J. Ji, W. C. Cooper, D. B. Dreisinger and E. Peters, *J. Appl. Electrochem.*, **25**, 642 (1995).

[17] T. Honda, K. Murase, T. Hirato and Y. Awakura, *J. Appl. Electrochem.*, **28**, 617 (1998).

[18] R. C. Wolfe, K. G. Weil, B. A. Shaw and H. W. Pickering, *J. Electrochem. Soc.*, **152**, 82 (2005).

[19] G. Wittstock, M. Burchardt, S. E. Pust, Y. Shen and Ch. Zhao, *Angew. Chem.*, **46**, 1584 (2007).

[20] W. J. Albery and E. J. Calvo, *J. Chem. Soc. Faraday Trans.*, **79**, 2583 (1983).

[21] S. Hessami and C. W. Tobias, *AIChE J.*, **39**, 149 (1993).

[22] C. Deslouis, I. Frateur, G. Maurin and B. Tribollet, *J. Appl. Electrochem.*, **27**, 482 (1997).

[23] M. C. Henstridge, G. G. Wildgoose and R. G. Compton, *J. Phys. Chem. C*, **113**, 14285 (2009).

[24] M. C. Henstridge, G. G. Wildgoose and R. G. Compton, *Langmuir*, **26**, 1340 (2010).

[25] S. Vesztergom, N. Barankai, N. Kovács, M. Ujvári, P. Broekmann, H. Siegenthaler and G. G. Láng, *Electrochem. Commun.*, **68**, 54 (2016).

[26] S. Vesztergom, N. Barankai, N. Kovács, M. Ujvári, P. Broekmann, H. Siegenthaler and G. G. Láng, *J. Solid State Electrochem.*, **20**, 3165 (2016).

[27] P. Delahay, *J. Am. Chem. Soc.*, **74**, 3497 (1952).

[28] K. Nagel and F. Wendler, *Z. Elektrochem.*, **60**, 1064 (1956).

[29] Y. Kanzaki, K. Tokuda and S. Bruckenstein, *J. Electrochem. Soc.*, **161**, 770 (2014).

[30] G. K. H. Wiberg and M. Arenz, *Electrochim. Acta*, **159**, 66 (2015).

[31] J. Durst, A. Siebel, C. Simon, F. Hasch, J. Herranz and H. A. Gasteiger, *Energy Environ. Sci.*, **7**, 2255 (2014).

[32] E. B. Carneiro-Neto, M. C. Lopes and E. C. Pereira, *J. Electroanal. Chem.*, **765**, 92 (2016).

[33] V. G. Levich, *Physicochemical Hydrodynamics*, Prentice-Hall, Englewood Cliffs, New Jersey (1962).

[34] T. Erdey-Grúz and M. Volmer, *Z. Phys. Chem.*, **150**, 203 (1930).

[35] S. A. S. Machado and L. A. Avaca, *Electrochim. Acta*, **39**, 1385 (1994).

[36] W. H. Smyrl and J. Newman, *J. Electrochem. Soc.*, **118**, 1079 (1971).

[37] A. J. Bard and L. R. Faulkner, *Electrochemical Methods. Fundamentals and Applications*, John Wiley & Sons, New York (2001).

[38] J. Newman, *J. Phys. Chem.*, **70**, 1327 (1966).

[39] W. H. Press, S. A. Teukolsky, W. T. Vetterling and B. P. Flannery, *Numerical Recipes in C: The Art of Scientific Computing*, Cambridge University Press, Cambridge (1992).

[40] D. Britz and J. Strutwolf, *Digital Simulation in Electrochemistry*, Springer, Berlin–Heidelberg (2005).

[41] Z. Galus and R. Adams, *J. Electroanal. Chem.*, **4**, 248 (1962).

[42] R. M. Machado and T. W. Chapman, *J. Electrochem. Soc.*, **134**, 385 (1987).

[43] C. S. Hofseth and T. W. Chapman, *J. Electrochem. Soc.*, **139**, 2525 (1992).

[44] F. W. J. Olver, *Introduction to Asymptotics and Special Functions*, Academic Press, Cambridge MA (1974).

[45] S. Lengyel and B. E. Conway, pp. 339–398, B. E. Conway, J. O'M. Bockris and E. Yeager, eds., *Comprehensive Treatise of Electrochemistry*, Plenum Press, New York (1983).

[46] S. Cukierman, *Biochim. Biophys. Acta*, **1757**, 876 (2006).

[47] D. G. Leaist and B. Wiens, *Can. J. Chem.*, **64**, 1007 (1986).

[48] D. Muñoz-Santiburcio and D. Marx, *Nat. Commun.*, **7**, 12625 (2016).

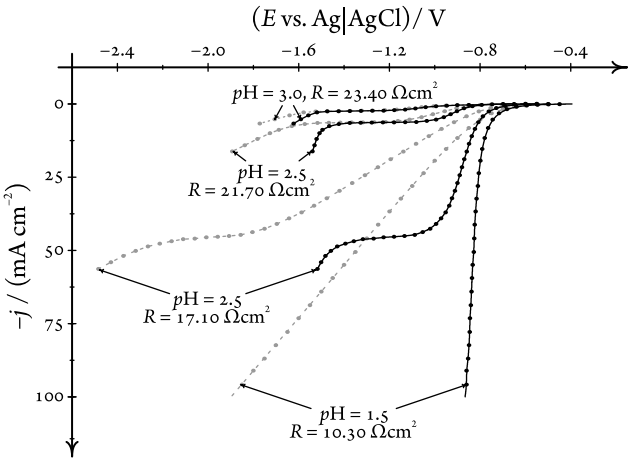

Figure 1: Stationary polarization curves measured on a Ni RDE immersed into solutions of different pH. Dots represent measured values, curves were created by spline interpolation. Black curves and dots are corrected against uncompensated IR drop; grey curves and dots show raw measurement data. Resistance values used for the IR correction are shown in the figure. Rotation rate: $f = 1225$ min^{-1}.

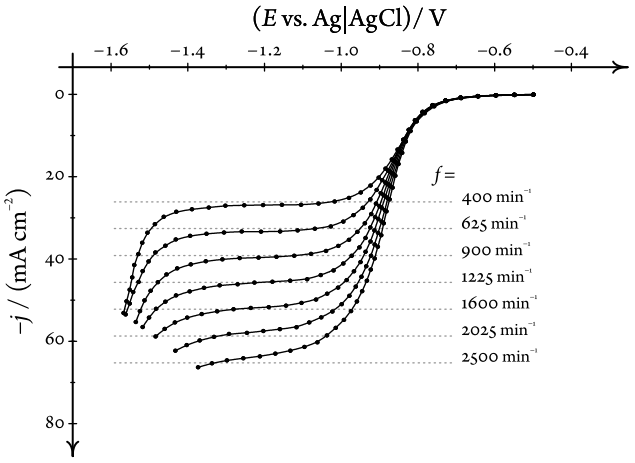

Figure 2: Stationary polarization curves measured at pH = 2.0 at different rotation rates f. Dots represent measured values, curves were created by spline interpolation. Dotted grey lines show limiting current levels at the different rotation rates, calculated from Equation (4) using the parameter values listed in Table 1.

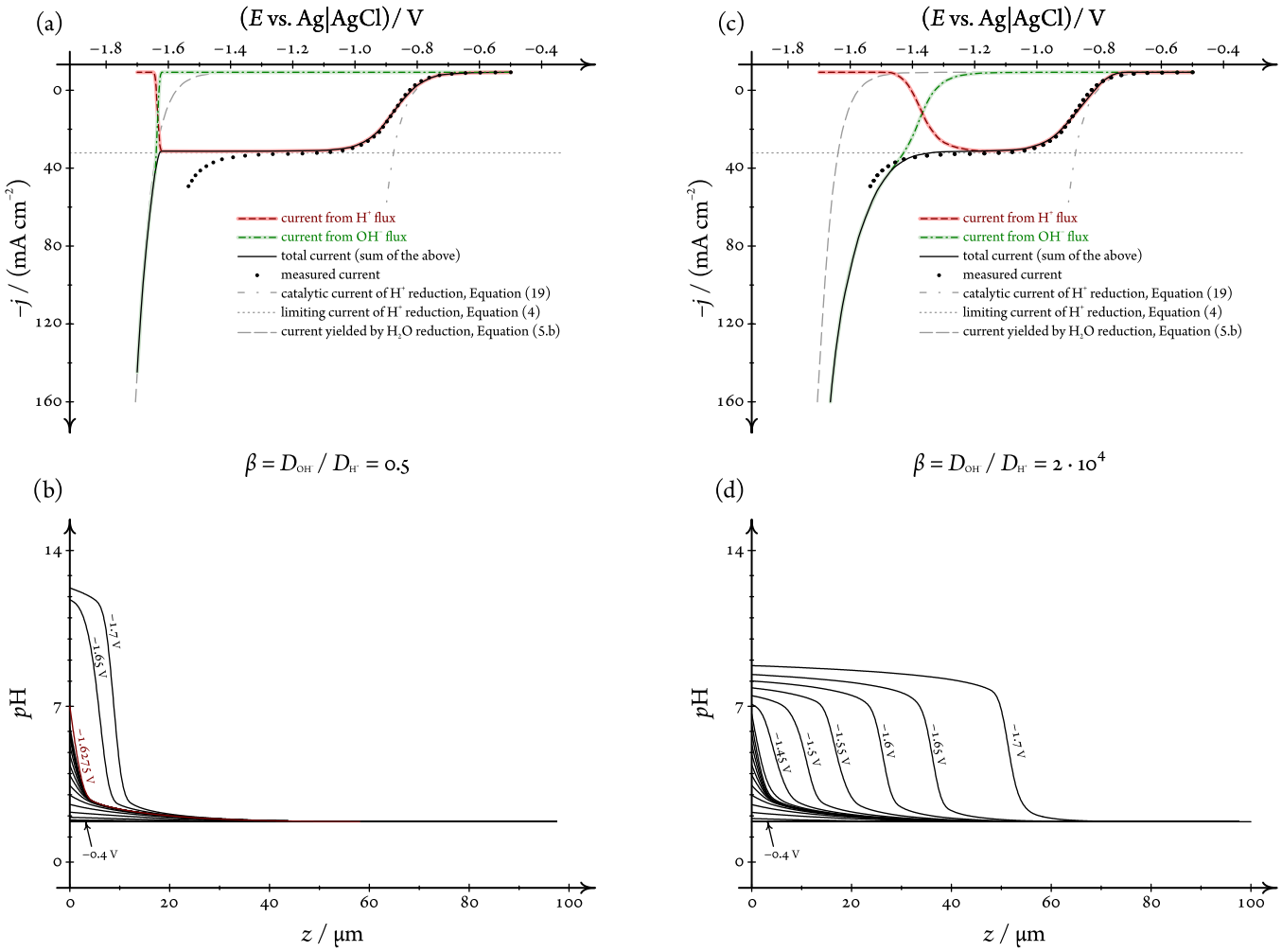

Figure 3: Results of digital simulation. Rotation rate: 900 min^{-1}, pH = 2.0 The polarization curves in (a) and (c) were calculated by summing the partial currents determined from the concentration gradients of H^+ and OH^-, as described by Equations (18.a)–(18.b). The two partial current densities, the catalytic (Equation (20)) and limiting (Equation (4)) current densities of H^+ reduction, as well as the current density yielded by the reduction of water molecules (Equation (5.b)) are also plotted, see the legend. Measured data are shown for comparison. In (b, d) stationary pH profiles are plotted for different values of the electrode potential (some are marked on the graph). The results shown in (a, b) were obtained by using a common literature value[30] of the $\beta = D_{OH^-}/D_{H^+}$ ratio of 0.5 while the results (c, d) were generated by using a much higher β value of $2 \cdot 10^4$. Other parameter values are listed in Table 1.

Table 1: Parameter values used in calculations at different levels of pH. Parameters marked with an asterisk are fixed; the rest of the values were determined by non-linear curve fitting (see Figure 5.

Symbol	**Definition**	**Value at**		**Unit**
		$p\mathbf{H} = 2.0$	$p\mathbf{H} = 2.5$	
$c^{\infty}_{\mathrm{H}^+}$	bulk concentration of H^+ ions	15.378	2.017	mmol dm^{-3}
D_{H^+}	diffusion coefficient of H^+ ions	9.171	9.804	10^{-5} cm^2 s^{-1}
E_1^{eq}	equilibrium potential, Reaction (1)*	−0.341	−0.370	V
k_1	reaction rate coefficient, Reaction (1)	2.788	1.633	10^{-7} cm s^{-1}
α_1	charge transfer coefficient, Reaction (1)	0.550	0.568	—
E_2^{eq}	equilibrium potential, Reaction (2)*	−1.169	−1.198	V
k_2	reaction rate coefficient, Reaction (2)	8.440	0.625	10^{-12} mol s^{-1} cm^{-2}
α_2	charge transfer coefficient, Reaction (2)	0.598	0.861	—
ν	kinematic viscosity*	»	0.01	cm^2 s^{-1}
T	temperature*	»	298.15	K

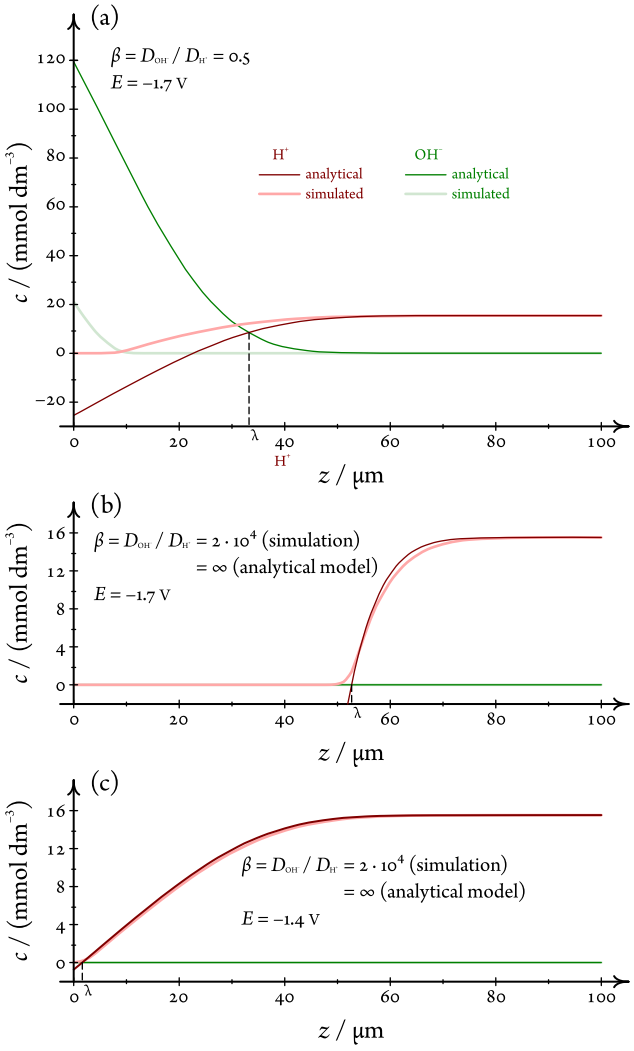

Figure 4: Concentration profiles determined by simulation (described in Section 4.1) and by the analytical approach of Section 4.2. The electrode potential and the ratio of diffusion coefficients β have different values in (a)–(c) as shown; $p\mathrm{H} = 2.0$, $f = 900\ \mathrm{min}^{-1}$. Further parameters are listed in Table 1.

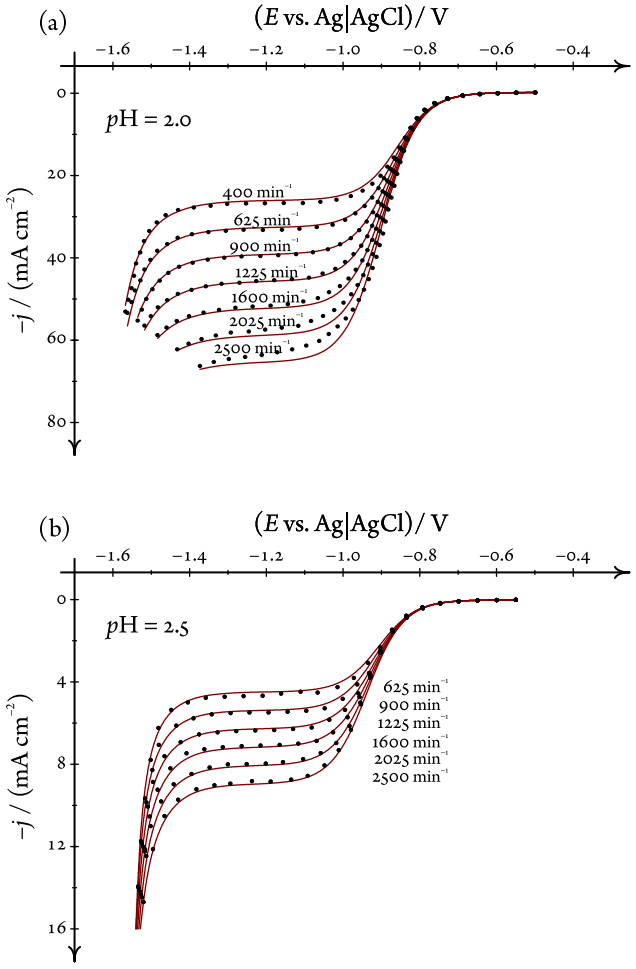

Figure 5: Stationary polarization curves measured on a Ni RDE immersed into a $p\mathrm{H} = 2.0$ (a) and a $p\mathrm{H} = 2.5$ (b) solution. The applied rotation rate f is varied as shown. Dots represent measured values, curves were created by non-linear curve fitting using the Levenberg–Marquardt method[39] and Equation (28). The parameter values given in Table 1 were determined by this fitting.

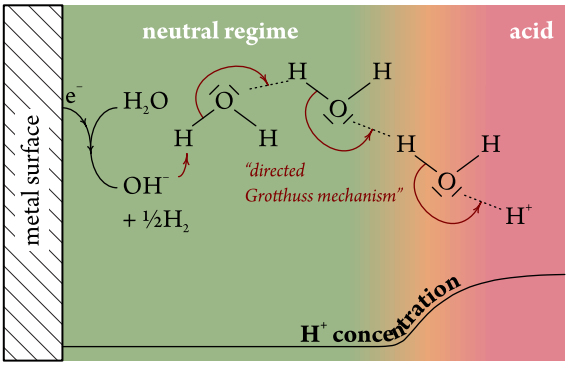

Figure 6: Scheme of a "directed Grotthuss mechanism" explaining the establishment of a neutral near-surface solution layer when water reduction takes place at the interface. It seems plausible to assume an extremely fast bond hopping mechanism between OH^- ions, created at the interface, and the large concentration of H^+ ions in the acidic bulk. This mechanism can account for the large (practically infinite) apparent diffusion coefficient of OH^- ions.